LIQUID CRYSTALS, VOL. 30, NO. 12, DECEMBER 2003, 1377–1390

Taylor & Francis
Taylor & Francis Group

Electric field-induced nucleation and growth of focal-conic and stripe domains in a smectic A liquid crystal

SHILA GARG*, KIRSTIN PURDY, ERICA BRAMLEY
Department of Physics, The College of Wooster, Wooster, OH 44691, USA

I. I. SMALYUKH and O. D. LAVRENTOVICH
Chemical Physics Interdisciplinary Program and Liquid Crystal Institute, Kent State University, Kent, OH 44242, USA

(*Received 23 June 2003; accepted 31 July 2003*)

We have studied the electric field-induced first order transition from a homeotropic smectic A structure to a polydomain texture that occurs through the nucleation of toric focal-conic domains (TFCDs). The process involves two steps: first, nucleation of TFCDs of a size larger than a critical radius a^*, and then a steady growth of TFCDs to a secondary critical radius a^{**}, when surface anchoring effects become dominant and cause a transition from a circular TFCD to an elongated stripe domain (SD). Studies were performed for pure smectic A materials and for smectic A doped with kunipia nanoparticles. Non-destructive 3D imaging with fluorescence confocal polarizing microscopy showed that field-induced TFCDs can nucleate in the smectic A bulk. Clay particles reduce the energy barrier for nucleation as they distort the smectic A layers and thus increase the ground state energy. Simple elastic models of the TFCD and SD allow us to describe the qualitative features of the observed phenomena.

1. Introduction

When a liquid crystal is subjected to a sufficiently strong electric or magnetic field, it can undergo structural transitions. Field-induced transitions are the fundamental property of liquid crystals that makes them media of choice for various display devices. The features of the transitions are determined by the type of ordering in the liquid crystalline medium and are very different for, say, nematic (N) and smectic A (SmA) liquid crystals. As it is well known, both the N and the SmA phases possess a uniaxial orientational order: long axes of molecules are on average oriented along one direction called the director **n**. In addition, the SmA phase is characterized by a quasi-long range 1D translational order along the director **n**. The latter is caused by periodic modulation of density which is absent in the N phase. When a SmA is subjected to an external field, the structural deformations are restricted by the requirement to preserve the thickness of layers close to its equilibrium value, which is of the order of the extended length of one molecule. As a result, the director field, which is perpendicular to smectic layers, prefers to splay rather than to twist or to bend, as pure splay deformations do not violate the equidistance of layers.

There is a broad class of equidistance-preserving configurations of layers called 'focal-conic domains' (FCDs). In FCDs, the layers fold around two confocal defect lines, either an ellipse and hyperbola or two parabolae; see, for example, the recent review [1]. The ellipse–hyperbola FCDs are often seen to degenerate into an axially symmetric structure, which we will call, following [1], a toric FCD (TFCD), with the ellipse replaced by a circle and the hyperbola replaced by a straight line passing through the centre of the circle. It has been reported [2, 3] that TFCDs are responsible for the field-induced structural transitions in the SmA slabs with an initially planar stack of unperturbed parallel layers. Since the director is perpendicular to the bounding plates, such a configuration can also be called a homeotropic SmA slab.

The appearance of TFCDs is a structural transition of the first order in which the system has to overcome a significant energy barrier for the TFCD embryo to become a viable growing nucleus of the reoriented phase [2, 3]. Therefore, such a transition can be facilitated by irregularities of the cell, such as surface roughness, mechanical impurities, etc. [3]. In this paper

*Author for correspondence; e-mail: sgarg@wooster.edu

Liquid Crystals ISSN 0267-8292 print/ISSN 1366-5855 online © 2003 Taylor & Francis Ltd
http://www.tandf.co.uk/journals
DOI: 10.1080/02678290310001621886

we study the structural features of nucleation and the initial growth of TFCDs caused by the electric field in a homeotropic cell with a SmA material that is doped with nanoparticles.

Li and Lavrentovich [2] investigated the scenario of the electric field-induced transition in a geometry similar to the present study, but for an undoped SmA material. They demonstrated that the transition is a two-step process. During the first step, as the voltage gradually increases, TFCDs of micron or submicron size a^* nucleate at different sites in the cell. These sites have either bulk or surface imperfections. Upon further field increase, the radius a of the TFCD increases, but only to some critical radius a^{**}, of the order of the cell thickness h. At $a > a^{**}$, the TFCD changes into a stripe domain (SD); the object looses its circular symmetry. Thus a field-induced stable TFCD in the restricted geometry of a homeotropic cell has two characteristic sizes: the minimum a^* size below which a TFCD embryo is unstable with respect to the unperturbed configuration of flat smectic layers, and a maximum size a^{**} above which the TFCD is unstable with respect to a SD. The two steps in the TFCD growth are controlled by different contributions to the free energy of the system [2, 3]. The first step, when $a^* < a < a^{**}$, is controlled mainly by (a) dielectric coupling energy of the anisotropic SmA phase and the electric field, (b) elastic energy of deformations in the TFCDs, and (c) energy of distortions around imperfections in the bulk of the material or at the surfaces of the cell. During the second step, $a > a^{**}$, the surface anchoring of the smectic layers at the bounding plates of the cell begins to play an increasingly significant role since TFCDs of large size inevitably require large deviations of layers from their initial orientations at the boundaries (parallel to the confining walls of the cell); non-zero surface anchoring leads to the morphological TFCD–SD change [2].

Nanoparticles in the liquid crystal might serve as nucleation sites along with other irregularities, such as spacers and the air–liquid crystal interface at the edge of the cell. The goal of this project is to investigate the initial growth of the TFCD until it reaches the critical diameter a^{**} before the transition to the striped phase takes place, and also to monitor the growth of SD at scales larger than a^{**}. Both these processes were monitored for both pure SmA material and for SmA doped with small kunipia particles.

2. Experimental technique

The cells were assembled from flat glass plates covered with electroconductive thin layers of indium tin oxide (ITO). To align the director homeotropically, the ITO layers were treated with weak solutions of lecithin in hexane (0.2% by weight). Mylar spacers of 36 μm were used to construct the cells. The cells were filled with SmA material CCN-47 (purchased from EM Industries). A polarizing microscopy test demonstrated good homeotropic alignment.

The experimental set-up is shown in figure 1. An Instec hot stage was used to maintain the cell at the desired temperature. CCN-47 has a room temperature SmA phase and the N–SmA transition temperature is 30.7°C. We chose to conduct the experiments at fixed temperature intervals from the transition temperature measured each time. We chose 1°C and 7°C below the N–SmA transition temperature as the experimental temperatures for pure CCN-47 cells.

A second set of cells was filled with CCN-47 doped with kunipia-f nanoparticles, which are tiny clay disks. Kunipia-f is a clay mineral that has a layered structure of aluminosilicates of formula $[(OH)_4Si_8(Al_{3.34}Mg_{0.66})O_{20}-Na_{0.66}]$. The layered structure is broken down into disks that have a 1 nm thickness and about a 100 nm diameter [4]. The kunipia-f particles were obtained from Toyota Central R & D Labs. After this procedure, 99.5 wt% of CCN-47 was mixed well with 0.5 wt% of the kunipia before a cell is filled. For these doped cells, the N–SmA transition temperatures were about a degree lower than the pure cells. We conducted the critical radius measurements at 1°C and 6°C below the N–SmA transition temperature.

To determine the growth up to the critical maximum radius a^{**} of the TFCD, a ramp rate of $1.3 \times 10^{-3}\,\mathrm{V\,s^{-1}}$ was used at an a.c. frequency of 1500 Hz until a threshold voltage was reached; at this threshold voltage ramping was stopped and the voltage held constant. The threshold voltage was taken to be the point at which the TFCDs started to nucleate and grow symmetrically, see figure 2 (*a*). The TFCD continued to grow beyond this threshold point until it reached its critical radius a^{**} and then deviated from being circularly symmetric when the subsequent transition to SD occurred. The growth of the TFCD to the critical radius a^{**} and the transition into the SD were monitored. The cell was observed through a polarizing microscope equipped with a CCD camera. A stop motion video capture sent digital data to an Apple video card in a Power Macintosh at a rate of 30 frames/min. The data was analysed using the software NIH Image 1.61. The size (characteristic length) of the SD was measured in three different directions, labelled by the angle between the direction of measurement and the horizontal axis in the polarizing microscope videoframe.

Experimentally, the challenge is to monitor the nucleation and the initial growth of the focal-conic domain before external changes initiated in the edge

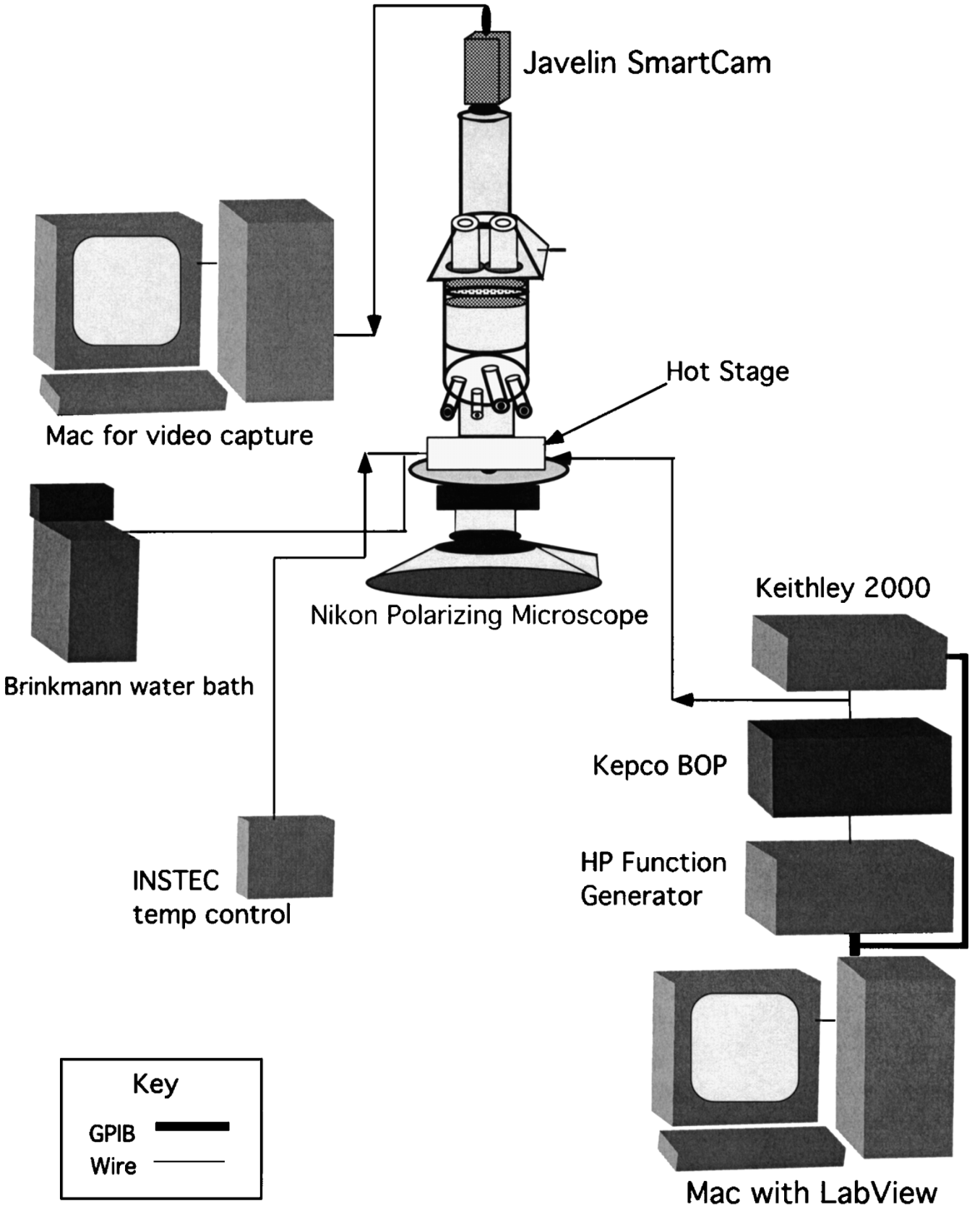

Figure 1. Experimental set-up.

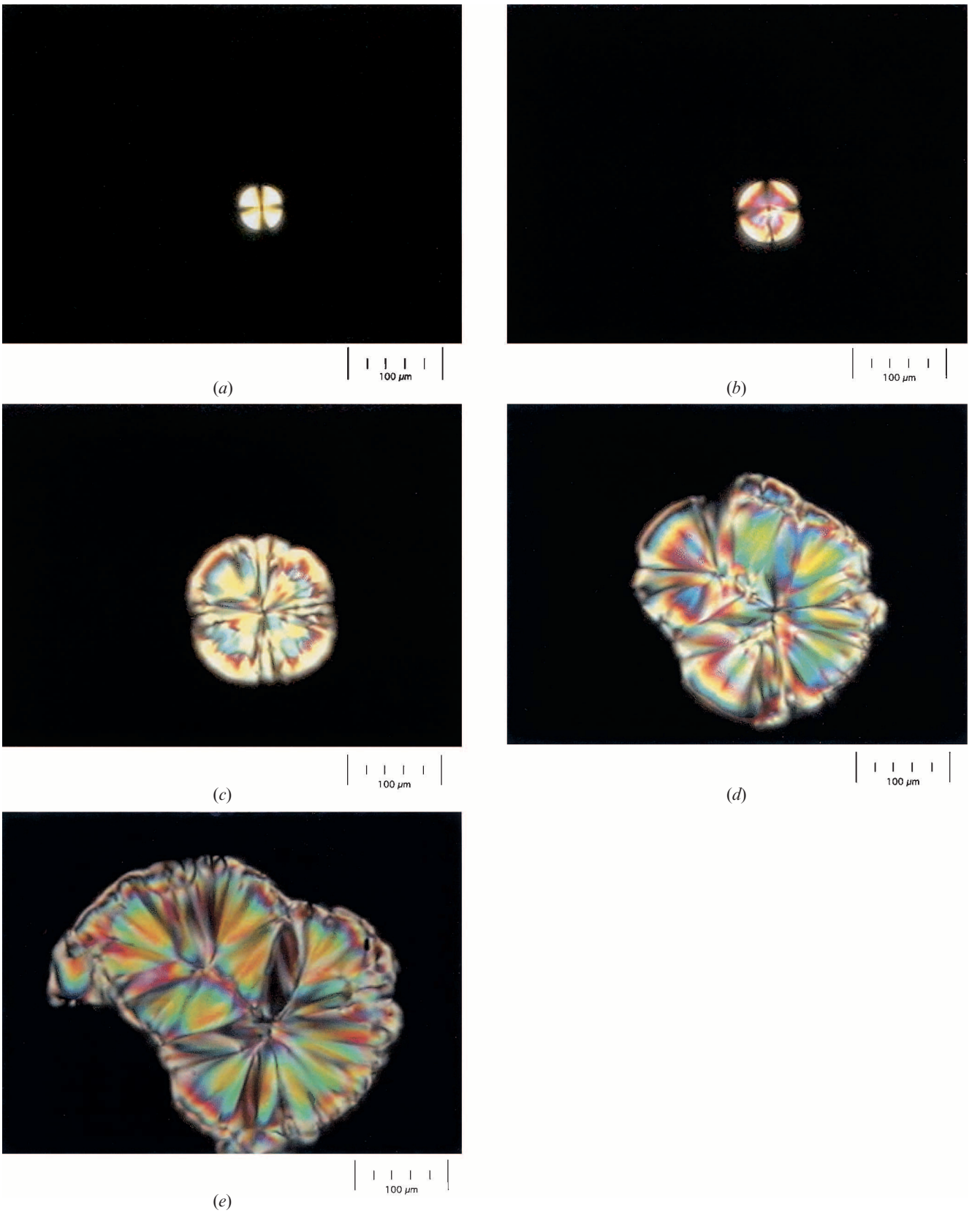

Figure 2. Nucleation and growth of a TFCD in a homeotropic cell of CCN-47 at 29°C. Starting with (*a*) the voltage was held constant at 52.510 V for all frames. (*a*) $t=0$ s; (*b*) $t=25$ s; (*c*) $t=50$ s; (*d*) $t=95$ s; (*e*) $t=100$ s.

region. Li and Lavrentovich [2] observed that the voltage at which nucleation occurs at different sites was different depending on the imperfections at the sites. Thus, the ramp rate of the voltage needs to be optimized. Several trials were performed to locate an appropriate site of a TFCD as well as the relevant voltage range. Each time the TFCDs nucleated and progressed to the SDs, the cell was heated to 70°C (at which the SmA material is in the isotropic phase) and cooled back to the homeotropic state. This initial growth and stabilization of the domain is a fairly slow process; the size of the FCD increases with increasing voltage until a critical radius a^* is reached and the domain becomes stable. Ramping of the voltage is continued until a threshold voltage is reached; it is held constant until the second critical radius a^{**} is reached and the transition to SD takes place. Once the TFCD transforms into a SD, the growth rate of the striped domain becomes very rapid.

3. Results

Figures 2 (*a–e*) show a typical TFCD, its initial growth, nucleation and transition to SD. Figures 3 (*a*) and 3 (*b*) are the growth graphs of a TFCD from a domain size smaller than the critical radius ($a < a^{**}$) at two different temperatures; the data points after the critical radius is reached show the growth of the striped domain. Figure 3 (*a*) is at a lower temperature (ΔT from N–SmA transition = 7°C) than 3 (*b*) ($\Delta T = 1$°C) and the growth rate at the lower temperature is not linear with time. Figure 3 (*b*) clearly shows a linear trend for the initial growth process after nucleation. In both figures 3 (*a*, *b*), the voltage ramping was stopped after the nucleation of TFCD, and the growth of the TFCD was monitored as well as the transition to SD and its growth to a certain extent. The change in growth rate takes place after the critical radius is reached at approximately 60 μm.

Figure 4 compares the radius of TFCD of pure CCN-47 and the doped CCN-47 at the same voltages. Data shown here were collected with the intent of determining the critical radius more carefully. A possible site of TFCD was identified by trial runs and this was monitored from zero voltage until there is nucleation of a TFCD.

Figure 5 is the graph of the initial growth of a SD in the doped cell as a function of time. The SD is initially an irregularly shaped circle, which elongates as it grows. By measuring its radial size along three directions, we obtain a sense of its non-uniform growth as well as shape. The growth dynamics of domains at the lower temperatures in both pure and doped cell seem similar. They could be described as step-like processes. However, in the pure cell at higher temperature (closer to the N–SmA transition), the growth appears linear. In the doped cell at the higher temperature (i.e. close to the N–SmA transition), the growth is still step-like. It is clear from figure 4 that the critical radius a^{**} is somewhat higher for the doped material. Note that the experimental data on a^{**} vary in a broad range, from about 10 μm (pure SmA material at relatively low temperature 22°C in figure 4) to 50–70 μm (for a higher temperature of 29°C, as in figure 2). This effect might be related to the temperature dependence of parameters such as the surface anchoring strength, as discussed later (see figure 10). The other significant observation is that the voltage needed for the transition to SD is relatively low, 73 V for the doped cell, 93 V for the pure cell, see figure 4.

Let us consider the basic features of the first step of the transition, namely, nucleation and growth of the circular TFCD. According to [3], nucleation and expansion of a TFCD strongly depend on whether the TFCD base is located at the bounding substrate, in the bulk of the cell or outside the cell (virtual singularities), see figure 6. Therefore, it is important to verify the location of the TFCD experimentally; the only adequate technique is that of fluorescence confocal polarizing microscopy (FCPM) [5].

4. Fluorescence confocal polarizing microscopy

Conventional polarizing microscopy does not allow one to decipher unambiguously the location of the TFCD's base since the technique essentially produces two-dimensional images by integrating the pattern of birefringence over the thickness of the cell. Recently, it has been proposed [5] that FCPM can be employed to visualize the 3D patterns of the director field. The essence of the technique is as follows.

The liquid crystal is doped with fluorescent molecules whose orientation is dictated by the local orientation of the liquid crystal. A highly focused polarized laser beam scans through the sample, each time illuminating only a small ($\sim 1\,\mu m^3$) volume. The fluorescent light is detected through a pinhole to discriminate against the regions above and below the selected volume. Light absorption and fluorescence both depend on the orientation of dye molecules with respect to the polarization of the light, and thus allow one to reconstruct the three-dimensional pattern of liquid crystal orientation [5]. The maximum fluorescence is detected when the polarization of light is parallel to the director (provided the transition dipole of the fluorescent molecules is along the director) [5]. In our experiments, we used a fluorescent dye *N*, *N*′-bis(2,5-di-*tert*butylphenyl)-3,4,9,10-perylenedicarboximide (BTBP). The dye was added to CCN-47 in quantities of 0.01 wt %, well below the solubility limits; nanoparticles were present in these

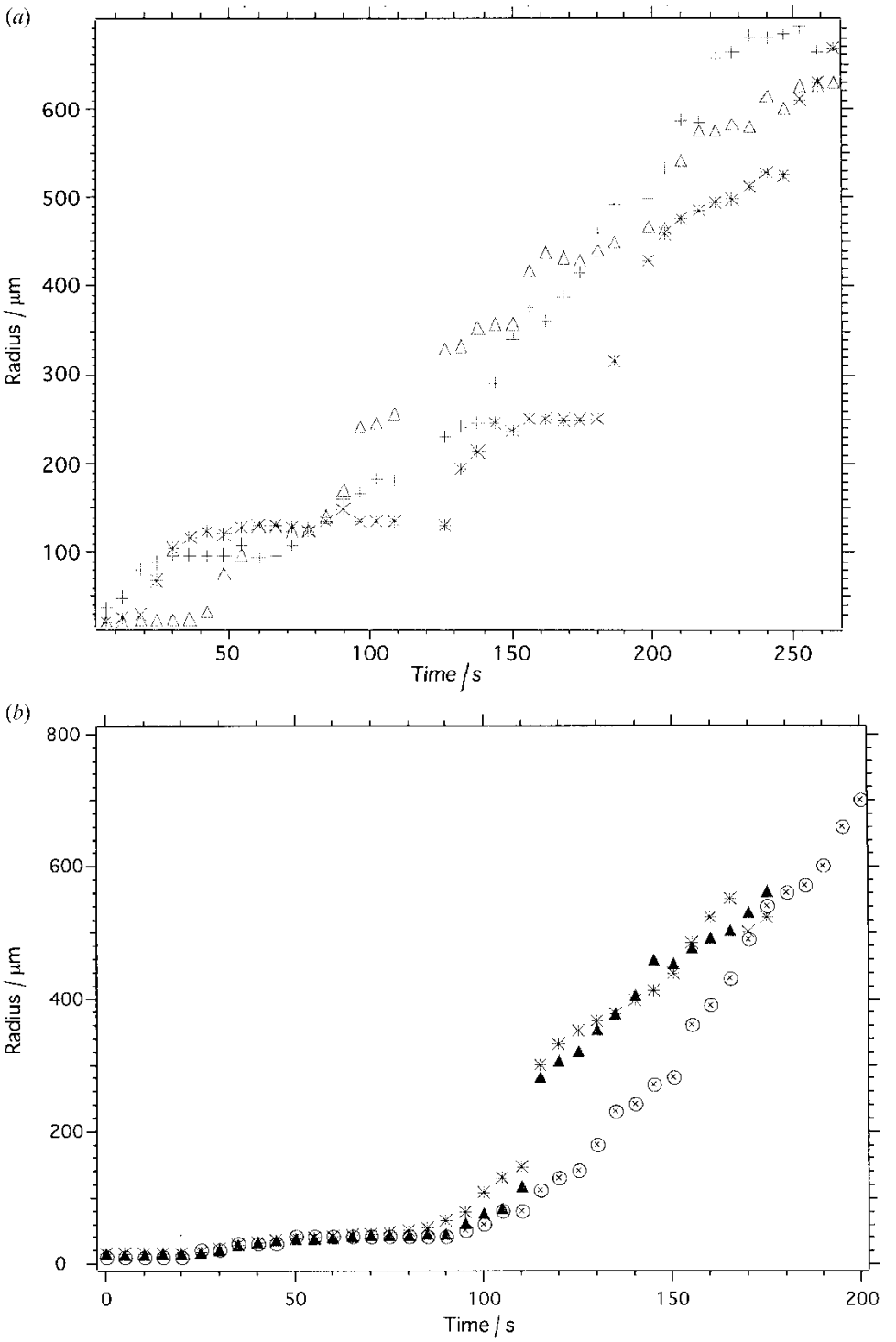

Figure 3. (*a*) Growth of stripe domain in pure CCN-47 at 22°C ($\Delta T = 7$°C). Symbols refer to measurements in three different directions from a horizontal line: + 145°; ✳ 225°; △ 320°. (*b*) Growth of TFCD and subsequently the stripe domain at 29°C ($\Delta T = 1$°C) in pure CCN-47. Symbols refer to three different measurements with respect to the horizontal: ▲ 45°, ✳ 135°; ⊗ 325°. Initial growth rate of TFCD: 0.428 μm s^{-1}; average rate of growth of SD: 6.59 μm s^{-1}. Voltages were held constant for both (*a*) and (*b*).

experiments. The birefringence of CCN-47 is relatively low ($n_o = 1.4723$, $n_e = 1.5075$), which helps to maintain reasonable resolution of the imaging (about 1 μm).

The SmA cell was prepared in a manner similar to other experiments with kunipia particles; an electric field was used to create the TFCDs. In the FCPM, the

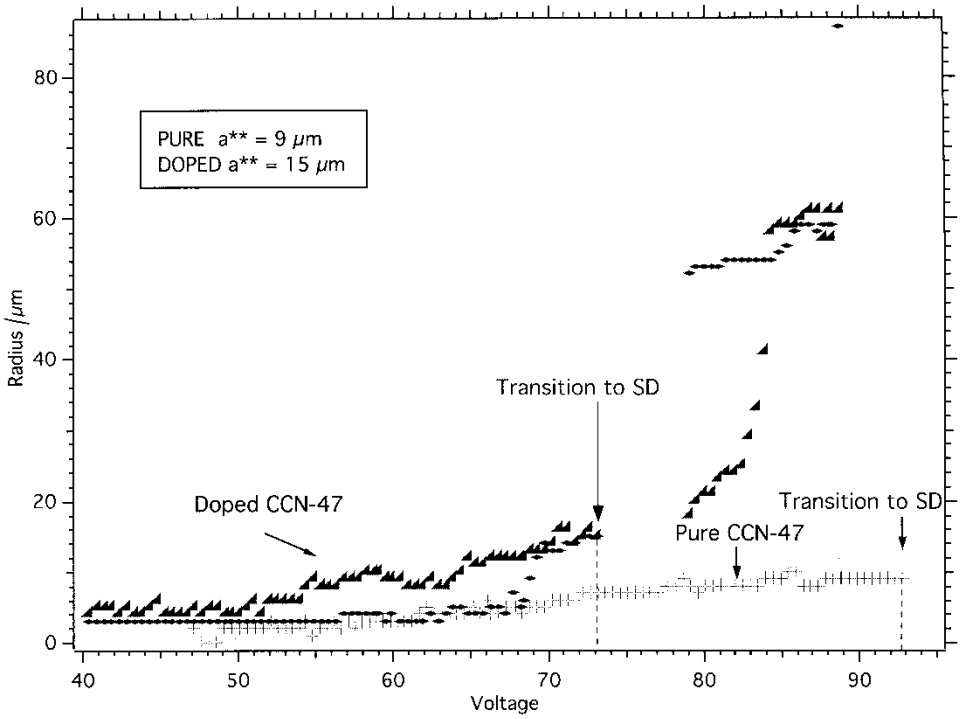

Figure 4. Determination of critical radius a^{**} in pure and doped CCN-47 at 22°C ($\Delta T = 7$°C for pure and 6°C for the doped).

laser beam scans the entire volume of the cell; the process takes a few seconds, or tens of seconds if the number of optical sections is large. Because of this limitation, we performed observations for the metastable TFCDs that remain in the cell after the electric field is switched off; their relaxation is slow and allows one to perform optical sectioning of the sample with sufficient resolution.

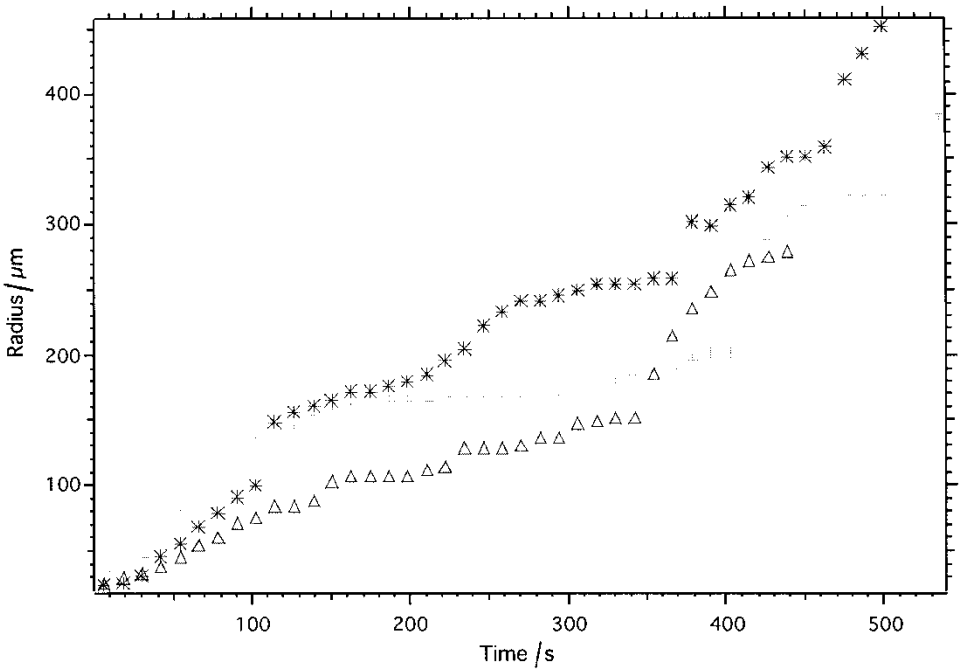

Figure 5. Growth of SD in doped CCN-47 at temperature 27°C ($\Delta T = 1$°C). Voltage held constant. Symbols refer to measurements in three different directions from a horizontal line: ✳ 38°, + 145°; △ 315°.

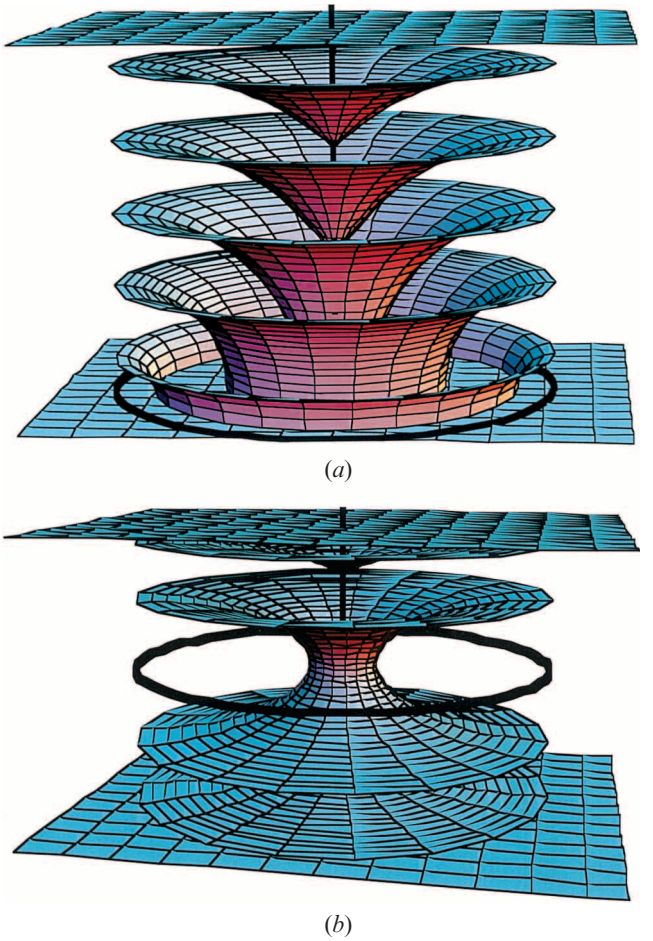

(*a*)

(*b*)

Figure 6. A TFCD in a smectic A liquid crystal nucleated (*a*) at the cell wall, (*b*) in the bulk of the cell.

Figure 7 shows the in-plane (*a*, *b*) and vertical (*c*) FCPM texture of the smectic cell with TFCDs. Since at the base of the TFCD the molecules are oriented horizontally, the base should be characterized by the maximum intensity of fluorescence. Figure 7 (*c*) clearly shows that the base of the TFCD is located in the bulk of the cell. This result is natural, as the homeotropic alignment at the bounding plates of the cell makes it difficult for the TFCD base to approach the boundaries.

5. Free energy considerations

5.1. *Nucleation of toric focal-conic domains*

The last result allows us to apply the model of bulk nucleation to the field-induced transition in the cells. According to [3], nucleation and growth of the TFCD from an ideal flat stack of layers is characterized by the free energy composed of elastic, dielectric and surface anchoring terms, all of which depend on the dimensionless order parameter $\rho = a/h$, where a is the radius of the domain and h is the thickness of the cell. Note that ρ gives a measure of the maximum layer tilt at the bounding surface with respect to the plates; this tilt θ changes from 0 at the periphery of the TFCD (where the layers become parallel to the plates) to its maximum value $\theta = \arctan(2a/h)$ at the points where the rotation symmetry axis of the TFCD crosses the bounding plates.

We use the following free energy functional for the sum f_b of bulk elastic and dielectric energy densities:

$$f_b = \frac{1}{2}K(\sigma_1+\sigma_2)^2 + \bar{K}\sigma_1\sigma_2 + \frac{1}{2}B\gamma^2 - \frac{1}{2}\varepsilon_0\,\varepsilon_a(\mathbf{E}\cdot\mathbf{n})^2 \tag{1}$$

where σ_1 and σ_2 are the two principal local curvatures of the smectic layers, K is the splay elastic constant, $\bar{K}$ is the saddle–splay elastic constant, B is the compressibility modulus, ε_0 is the permittivity of free space, $\varepsilon_a = \varepsilon_\parallel - \varepsilon_\perp < 0$ is the dielectric anisotropy of SmA, $\varepsilon_\parallel$ and $\varepsilon_\perp$ are the relative electric permittivities (the subscripts refer to the director **n**), **E** is the applied electric field and **n** is the director. The surface anchoring of lamellar phases is generally different from the anchoring of nematic liquid crystals, as not only the director, but also the layered structure, is strongly distorted near the bounding substrate [2]. For the nucleation problem, $\rho \ll 1$, the surface anchoring at the bounding plates can be neglected, as we have seen experimentally that the TFCDs nucleate in the bulk and do not disturb the layered structure near the bounding plates; however, it should be included in the discussion of the TFCD–SD transformation, as discussed later.

Using the model [3] developed for the magnetic field effect, and rewriting equation (17) in [3] in terms of the electric field (and neglecting the non-local field effects), one obtains the excess energy associated with the appearance of a TFCD (as compared with the energy of the uniform state under the action of the same electric field):

$$\begin{aligned}\Delta F = 2\pi Kh\rho\Bigg[&\frac{\pi}{2}\ln 2 + L(\operatorname{arcctg} 2\rho) \\ &+ 2\operatorname{arcctg}2\rho\left(\ln\frac{h\rho}{\xi} - 2\right) \\ &+ \operatorname{arctg}2\rho\,\ln\frac{\rho h}{\xi(4\rho^2+1)^{\frac{1}{2}}} - \frac{1}{\rho}\ln\left(1+4\rho^2\right)\Bigg] \\ &- 2\pi\bar{K}h\left[\pi\rho - 2\rho\operatorname{arctg}2\rho + \ln\left(1+4\rho^2\right)\right] \\ &+ \frac{\pi}{24}\varepsilon_a\varepsilon_0 E^2h^3\left[8\rho^2 - 6\rho\operatorname{arctg}2\rho\right. \\ &\left.+ \ln\left(1+4\rho^2\right) + 4\pi\rho^3 - 8\rho^3\operatorname{arctg}2\rho\right]\end{aligned} \tag{2}$$

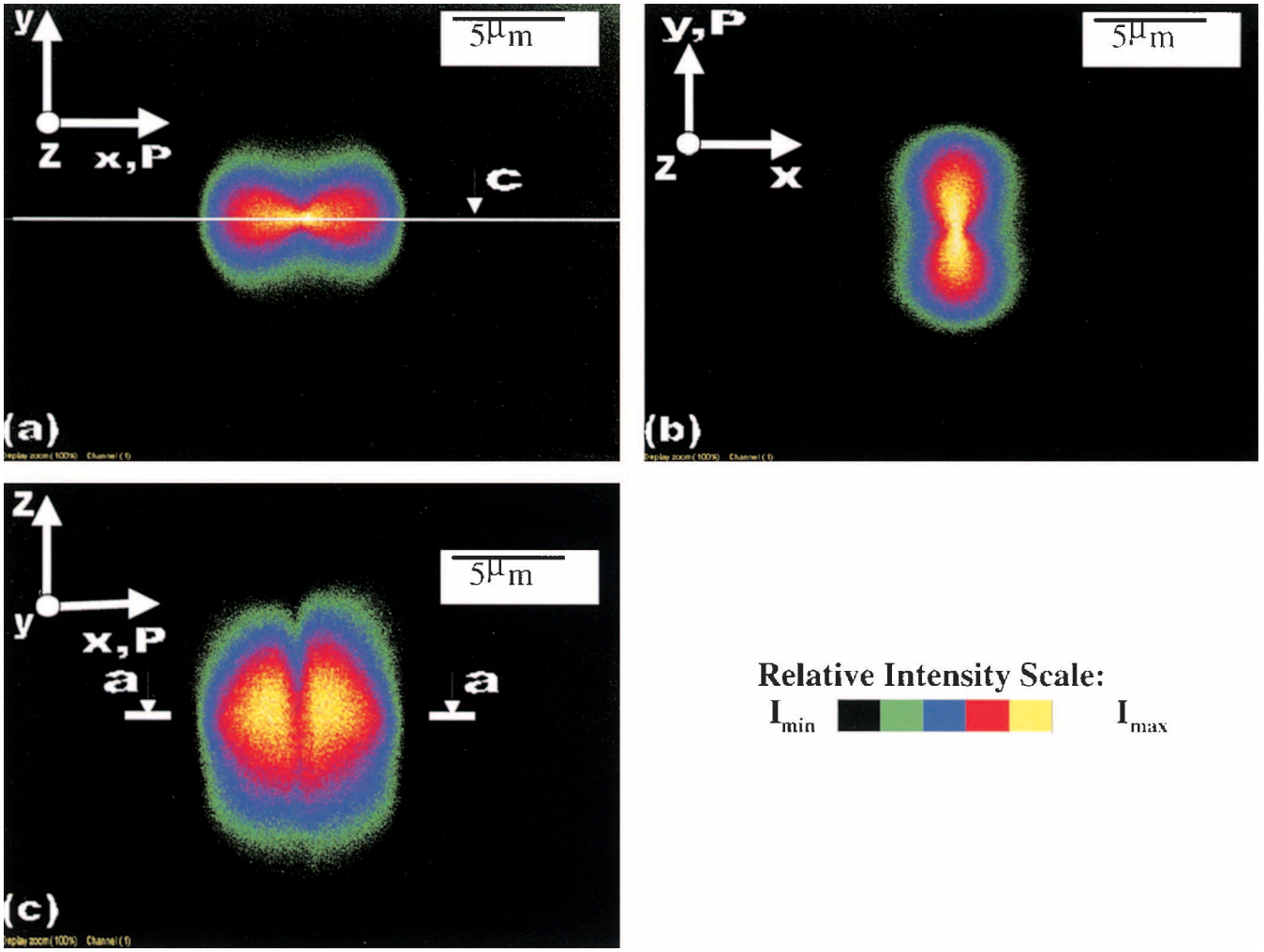

Figure 7. Fluorescence confocal polarizing microscopy texture of a field-induced focal-conic domain in the smectic A phase of CNN-47 doped with kunipia particles. Frames (*a*) and (*b*) represent horizontal (*x*, *y*) optical slices of thickness 1 μm taken from the middle plane of the cell that contains the base of the domain. Polarization of light is parallel to the *x*-axis in (*a*) and to the *y*-axis in (*b*). Line "c" shows the location of the vertical *xz* cross-section of the cell, depicted in frame (*c*). Frame (*c*) shows the vertical (*zx*) cross-section of the domain; lines "a" mark the location of frames (*a*) and (*b*). The maximum intensity of the fluorescent light is in the regions where $\hat{\mathbf{n}} \| \mathbf{P}$.

where ξ is the core radius of the circular defect and $L(x)$ is Lobachevskiy's function

$$L(x) = -\int_0^x \ln\cos t\,\mathrm{d}t = x\ln 2 - \frac{1}{2}\sum_{i=1}^{\infty}(-1)^{i-1}\frac{\sin 2ix}{i^2}. \tag{3}$$

Figures 8 (*a*) and 8 (*b*) show $\Delta F(\rho, E)$ as the function of the domain radius and the applied field, calculated using equations (2) and (3) with $h = 36\,\mu\mathrm{m}$ $K = 10^{-6}$ dyn, $\bar{K} = 0$, $\varepsilon_a = -10$ [2]. Lobachevskiy's function is calculated with accuracy up to the first 40 terms in equation (3), using *Mathematica* Version 4.2.

The free energy (2) can be expanded for small $\rho \ll 1$:

$$\Delta F = A_1\rho + A_2\rho^2 + A_3\rho^3 + A_4\rho^4 + \ldots \tag{4}$$

where the coefficients are

$$A_1 = 2\pi^2 Kh(\beta - 2 - \bar{K}/K). \tag{5}$$

Here $\beta = \ln(2h\rho/\xi) \approx const$ (for $a \gg \xi$ the logarithmic dependence is weak);

$$A_2 = 4\pi Kh\left(\ln\sqrt{2} - \beta - 3\right) \tag{6}$$

$$A_3 = \frac{\pi^2}{6}\varepsilon_0\varepsilon_a E^2 h^3. \tag{7}$$

The linear coefficient A_1 is always positive (otherwise the SmA planar state would not be stable). We will

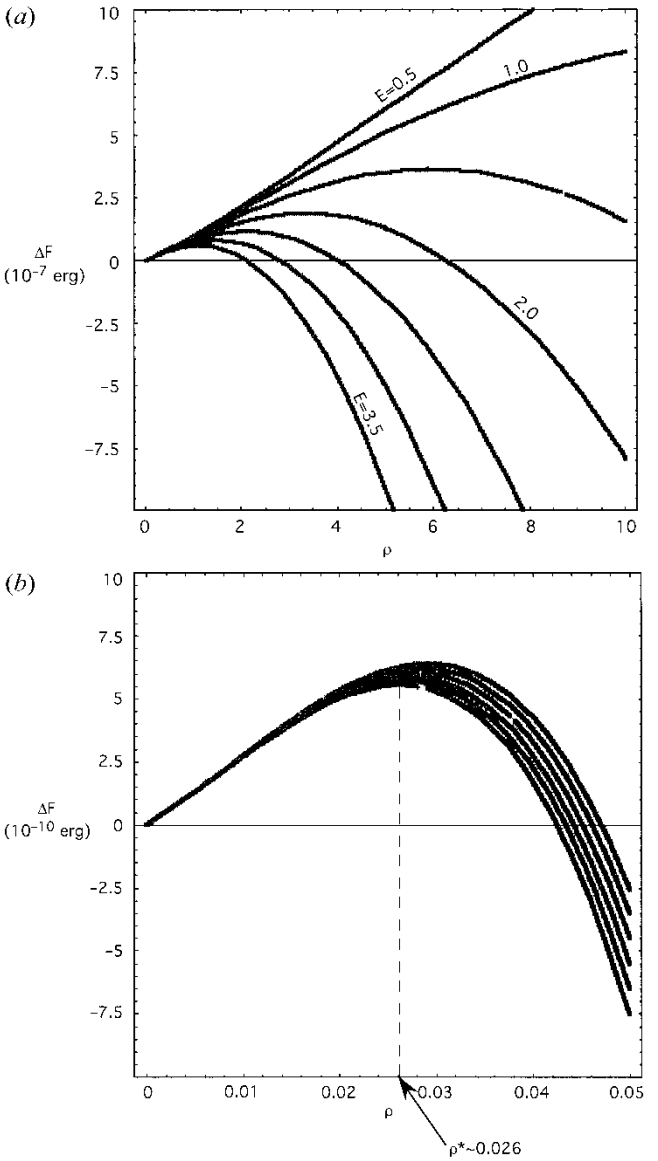

Figure 8. Free energy of the TFCD as a function of the dimensionless parameter $\rho = a/h$; plots are calculated using equations (2) and (3). (*a*) The different curves correspond to various E field values with units of statV cm^{-1}. (*b*) The region $\rho < 0.1$ is magnified with $E = 65$ to 70 statV cm^{-1}. ρ^* of 0.026 corresponds to a^* of 0.936 μm.

assume $\bar{K} = 0$. The third term A_3 is defined solely by the field contribution.

The dependences $\Delta F(\rho, E)$ for small ρ, figure 8 (*b*), clearly demonstrate the first order character of the transition. The function $\Delta F(\rho)$ goes through a maximum $\Delta F^* = \Delta F(\rho^*)$ at some critical radius ρ^* that defines the critical TFCD nuclei. Only the TFCDs of a sufficiently large radius $\rho > \rho^*$ transform the metastable uniform state into the stable defect state. The TFCDs with $\rho < \rho^*$ (embryos) are unstable and will decay.

The energy barrier that separates the two states is brought about by the *positive* leading elastic term in the expansion (4). This term scales practically *linearly* with ρ and this explains why the barrier always exists and is located in the region of relatively small ρ: the driving force, in accordance with equation (7), contributes only to the *cubic* (field) term.

TFCD nucleation could be observed over a reasonably short time if $\Delta F^* \leqslant 80 k_B T$, or $\Delta F^* \leqslant 3 \times 10^{-12}$ erg, see, for example, [3, 6, 7]. However, the typical barrier of TFCD nucleation proves to be higher. We assume the simplest situation: if the field is strong enough, $A_2/(A_1|A_3|)^{\frac{1}{2}} = \bar{\omega} \ll 1$. The barrier, located at

$$\rho^* \cong \frac{2}{Eh}\left[\frac{K(\beta - 2 - \bar{K}/K)}{\varepsilon_0|\varepsilon_a|}\right]^{\frac{1}{2}} \tag{8}$$

is

$$\Delta F^* \approx \frac{8\pi^2 K^{3/2}(\beta - 2)^{3/2}}{3(\varepsilon_0|\varepsilon_a|)^{\frac{1}{2}}E} \tag{9}$$

and remains quite high, to be surmounted by fluctuations $\Delta F^*_{BN} \sim 3 \times 10^{-12}$ erg only if the field is higher than 5.5×10^4 V cm^{-1} for our material, which is well above the field used in the experiments. Therefore, TFCD nucleation is a strongly heterogeneous process initiated by mechanical impurities. As shown in [3], these impurities distort the layers' structure and thus increase the energy of the ground (zero-field) state; this feature strongly reduces the energy barrier for nucleation. Within the frame of the model that assumes a set of dislocations around the mechanical particle of biconical shape of height $2l$ and radius R,

$$\Delta F^*_{impur} \cong \frac{8\pi^2 K^{3/2}}{3\sqrt{\varepsilon_0|\varepsilon_a|E}}(\beta - 2 - ld/2\pi\lambda\xi)^{3/2}. \tag{10}$$

Here $\lambda = (K/B)^{\frac{1}{2}} \approx d$ is the penetration length of SmA, d is the layer thickness. The last term in equation (10) decreases the energy barrier (and thus increases the possibility of TFCD nucleation) and can even make it disappear. The barrier might even disappear all together. If $d \sim \xi \sim \lambda \sim 30$ Å, $\bar{K} = 0$, $\beta \sim 4$–10, the last situation is satisfied for particles with height as small as $2l \sim (10$–$50)d$, i.e. $2l \sim (30$–$150)$ nm. It simply means that a bulk or surface irregularity of sufficient size can nucleate the TFCD even when the external field is absent. We expect that small aggregates of kunipia-f nanoparticles might serve as nucleation sites.

In the experiments, the growth of a TFCD was seen interrupted by other domains nucleated nearby. The

feature is the result of Friedel's 'law of impenetrability' which states that two TFCDs cannot penetrate each other [8, 9]. In other words, the interaction of two TFCDs is of steric nature [1, 9].

The growth of $a > a^*$ to $a = a^{**}$ in the pure material at 29°C appears to be fairly linear, figure 3 (*b*). Moreover this growth occurs at constant voltage. This behaviour is reminiscent of the Avrami model of classical kinetic theory [10]. According to this model, in first order transformations nuclei of the product phase grow to reach a critical size, dependent on time and temperature. The physical properties of importance are: (i) nucleation rate per unit volume, which is a function of the activation energy for the molecular migration involved in the transformation and the critical free energy barrier, and (ii) the growth rate of the product phase, which depends on the undercooling at the growth interface [11]. The dynamics of the expansion of TFCD and SD is an interesting subject worthy of further study. Below we discuss the most important event observed after the nucleation of the TFCDs, namely the transformation of the TFCDs into SD. Experimentally, the TFCDs that reach a^{**} loose their circular symmetry, figures 2 (*d*, *e*). The circular growth is replaced with a non-uniform expansion in the plane of the cell. We describe the SD as an elongating domain of a practically constant width $\rho_s = 2a/h$, where $a > a^{**}$. This constant width approximation neglects some variations in SD width that are caused primarily by the complex structure of their central part, which is the defect wall partially relaxed by smaller focal-conic domains [1, 9].

5.2. *Expansion through stripe domains*

To understand the transformation TFCD–SD that occurs when the radius of the domain exceeds some critical value ρ^{**}, one needs to compare the free energies of the TFCD and the SD. Qualitatively, the reason is that as the TFCD radius increases, the SmA layers makes an increasingly large angle, $\theta \to \pi/2$, with the bounding substrates; the surface anchoring cost hinders expansion of the TFCD above some critical size [2]. In contrast to a TFCD, a SD expands by elongation, while preserving the maximum value of the layers tilt $\theta = \arctan(2a/h) = \arctan \rho_s$ which is determined by the (nearly constant) width ρ_s of the SD. In the following, we calculate the free energy density of the SD as a function of its width and demonstrate that there is a particular width (at each value of the applied voltage) for which the 'line tension' of the SD becomes negative; such a SD will then elongate.

We employ the simple SD model shown in figure 9. The model is similar to that of the oily streaks in cholesterics [14], with the difference that the characteristic values of the material parameters (periodicity, anchoring strength, elastic constants) are different. The analysis reduces to calculation of the free energy of the vertical cross-section of the domain (energy per unit length) as the function of the applied field and the width of the domain. In other words, the calculations involve only the cylindrically distorted layers in figure 9 and not the layers at the end of the SD which are curved as half of a TFCD.

Inside the SD, one of the principal curvatures is zero, while another is $1/r$, where r is measured from the 1/2 disclinations at the left and right border of the SD. Using equation (1), we calculate the dielectric energy of a SD in an applied voltage U as

$$\begin{aligned}\Delta F_{\text{diel}} &= -\frac{\varepsilon_0 \varepsilon_a}{2}\left(\frac{U}{h}\right)^2 \left(\int\int \cos^2\theta r \, \mathrm{d}r \, \mathrm{d}\theta - 2ah\right) \\ &= -\frac{1}{4}\varepsilon_0 |\varepsilon_a| U^2 \left[1 - \left(1+\rho_s^2\right) \right. \\ &\quad \left. \times \arctan \rho_s + \frac{\pi}{2}\rho_s^2\right]. \end{aligned} \tag{11}$$

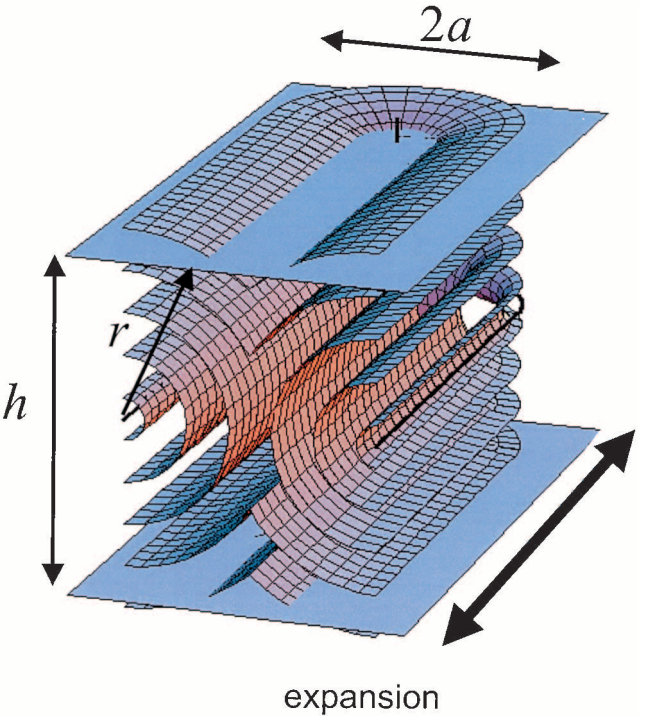

Figure 9. Schematic structure of the stripe domain with a semicircular FCD cupping the far end.

The curvature energy of layers forming U-turns inside the SD is

$$\Delta F_{\text{elastic}} = \pi K \ln\frac{\rho_s h}{2r_c} - 2K \arctan\rho_s \ln\rho_s + 2KL\left(\frac{\pi}{2} - \arctan\rho_s\right) + 2KL(\arctan\rho_s) \tag{12}$$

where r_c is the core radius of the disclination of strengh 1/2 running along the edge of the SD (figure 9).

The bend energy above must be supplemented by the core energy of the two side disclinations (which scale as $\sim K$ per unit length) and, most importantly, by the core energy of the wall. The wall defect at the vertical symmetry plane of the SD is a tilt grain boundary. The structure of the tilt wall is complicated, as it usually includes a whole hierarchy of secondary focal conic domains [1, 9]. The wall defect at the SD is even more complex, as the tilt angle between the two sets of smectic layers at the right and left parts of the SD changes from 0 (in the middle of the cell) to $2\arctan(2a/h)$ (at the bounding plates). To estimate the energy of the wall we assume, following [13, 2], that the elastic energy density at the wall is zero for $\theta_w = 0$, $\pi/2$, and a maximum for $\theta_w = \pi/4$, i.e. it is $f_{\text{wall}} \approx (KB)^{\frac{1}{2}} \sin 2\theta_w$; here θ_w is the angle between the plane of the defect wall and the SmA layers on either side of the wall. Integration over the area $2a \times h$ of the wall yields

$$\Delta F_{\text{wall}} \approx (KB)^{\frac{1}{2}} \rho_s h \ln\left(1 + \rho_s^{-2}\right). \tag{13}$$

Finally, as the layers are strongly tilted at the bounding plates, the anchoring energy cannot be neglected. The anchoring potential is assumed to be proportional to the number of smectic layers crossing the interface per unit area, $f_s \propto \sin|\theta|$ [2, 14]:

$$f_s \propto W \sin|\theta| \tag{14}$$

where $W = \alpha(KB)^{\frac{1}{2}}$ is the 'intrinsic anchoring coefficient' associated with the breaking of strongly titled layers near the substrates [2] and the unknown parameter α is of the order of 1 [14]; θ is the surface tilt of layers measured from their unperturbed horizontal orientation. Taking into account that the range of variation of the surface tilt is between $\theta = 0$ (at the edge of SD, where the layers smoothly transform into horizontal surfaces) and $\theta = \arctan\rho_s$ (at the vertical symmetry plane of SD), and integrating over the distance $2a$ at each of the two bounding plates, one obtains

$$\Delta F_s = 2hW\left[\left(1 + \rho_s^2\right)^{\frac{1}{2}} - 1\right]. \tag{15}$$

Collecting the relevant terms, $\Delta F = \Delta F_{\text{diel}} + \Delta F_{\text{elastic}} + \Delta F_{\text{wall}} + \Delta F_s$, one finds the free energy per unit length of the SD (as compared with the uniform texture in the electric field):

$$\begin{aligned}\Delta F_{\text{SD}} = &-\frac{1}{4}\varepsilon_0|\varepsilon_a|U^2\left[1 - \left(1+\rho_s^2\right)\arctan\rho_s + \frac{\pi}{2}\rho_s^2\right] \\ &+ \pi K \ln\frac{\rho_s h}{2r_c} - 2K\arctan\rho_s\ln\rho_s \\ &+ 2KL\left(\frac{\pi}{2} - \arctan\rho_s\right) \\ &+ 2KL(\arctan\rho_s) \\ &+ (KB)^{\frac{1}{2}}\rho_s h\ln\left(1+\rho_s^{-2}\right) \\ &+ 2hW\left[\left(1+\rho_s^2\right)^{\frac{1}{2}} - 1\right].\end{aligned} \tag{16}$$

The $\Delta F_{\text{SD}}(\rho_s)$ plots for different voltages and two different anchoring coefficients $W = 3.4 \times 10^{-3}$ and $5.5 \times 10^{-3}\,\text{J m}^{-2}$ are shown in figure 10 (*a*) and 10 (*b*), respectively. We used the following parameters: $K = 10^{-11}\,\text{N}$, $(K/B)^{\frac{1}{2}} = 5\,\text{nm}$, $\varepsilon_a = -10$, $h = 36\,\mu\text{m}$, $r_c = 1\,\text{nm}$. Note that at small voltages, $\Delta F_{\text{SD}}(\rho_s)$ is monotonically increasing, but at higher voltages, it acquires a non-monotonous behaviour with a pronounced minimum at a finite ρ_s. This minimum reaches a zero value $\Delta F_{\text{SD}}(\rho_s) = 0$ at $\rho_s = \rho_s^{**}$ when the voltage reaches $U^{**} = 73.2\,\text{V}$ for $W = 3.4 \times 10^{-3}\,\text{J m}^{-2}$, or $U^{**} = 92.45\,\text{V}$ for $W = 5.5 \times 10^{-3}\,\text{J m}^{-2}$; at any higher voltage, the energy becomes negative, which means that the SD will expand, increasing its length. Note that ρ_s^{**} is very sensitive to the voltage increase. For example, in figure 10 (*b*), raising the voltage from $U^{**} = 92.45$ to 93 V changes the value of ρ_s^{**} from 2.55 to 3.1. Moreover, as the voltage increases above U^{**}, the range of values of the SD width that corresponds to a negative line tension becomes rather large. For example, in figure 10 (*b*), raising the voltage only slightly from $U^{**} = 92.45$ to 93 V results in the broad range of the SD capable of extension, with width ranging from $\rho = 1.8$ to 5 (which corresponds to $30\,\mu\text{m} < a < 90\,\mu\text{m}$); SDs that are both wider and narrower than $\rho_s^{**} = 2.55$ can elongate. The shallow character of the minimum in the function $\Delta F_{\text{SD}}(\rho_s)$ explains highly irregular shapes of the domains after they reach the size ρ^{**}.

Note also that the critical radius ρ_s^{**} is sensitive to the polar anchoring coefficient W. Stronger anchoring and larger W imply a smaller ρ_s^{**}, as can be seen from equation (16) and from the comparison of figures 10 (*a*) and 10 (*b*). For example, $\rho_s^{**} = 2.6$ for a large $W = 5.5 \times 10^{-3}\,\text{J m}^{-2}$, but $\rho_s^{**} = 3.6$ for a smaller $W = 3.4 \times 10^{-3}\,\text{J m}^{-2}$, figure 10. As the anchoring

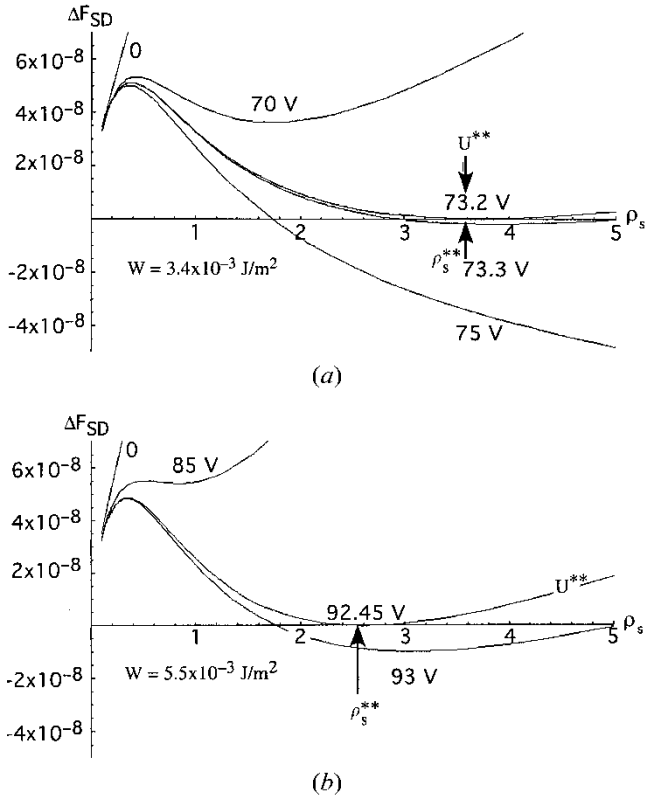

Figure 10. Free energy density per unit length of the SD as a function of the dimensionless width of the SD for different values of the applied voltage indicated at the plot, and for two different values of the surface anchoring strength: (*a*) $W=3.4\times10^{-3}\,\mathrm{J\,m^{-2}}$; (*b*) $W=5.5\times10^{-3}\,\mathrm{J\,m^{-2}}$.

coefficient in SmA strongly depends on the elastic constants, $W=\alpha(KB)^{\frac{1}{2}}$ in our model, one would expect W to decrease with temperature [2]. Therefore, ρ_s^{**} should depend on temperature and is likely to increase with temperature, which is consistent with our experimental data: a^{**} varies from about 10 μm at 22°C in figure 4 to 50–70 μm for the higher temperature of 29°C in figure 2. Such a trend is easy to understand. The very reason for the TFCD–SD transformation is the surface anchoring: if it is absent, $W\to0$, then $\rho_s^{**}\to\infty$ and the TFCD would expand indefinitely. In such an indefinitely expanding TFCD, the SmA layers eventually become perpendicular to the bounding plates, i.e. they deviate significantly from the original 'parallel' orientation that is stable at zero field. If W is finite, then such an expansion of TFCD costs too much surface energy and is replaced by a SD. A SD propagates by elongation while preserving its width ρ_s nearly constant; the maximum deviation of the layers from the anchoring-imposed orientation at the boundaries is limited, $\theta=\arctan\rho_s$, $\theta<\pi/2$.

The remaining issue is to determine whether the critical voltage U^{**} depends on the surface anchoring coefficient. Note first that at large values of $\rho_s\geqslant1$, the contribution of the elastic bend energy is extremely small as compared with the dielectric and anchoring energy. Furthermore, at the same scales, the wall energy is relatively small as compared with the anchoring energy (partly because the singularity can be relaxed by secondary focal-conic domains [9] and partly because the area of the wall is smaller than the area of the bounding plates at which the anchoring is broken). Therefore, the threshold voltage is determined mostly by the balance of the dielectric and surface anchoring terms in equation (16). The balance of these two terms for $\rho_s\geqslant1$ suggest a scaling of the type, $U^{**}\sim\left(\frac{Wh}{\varepsilon_0|\varepsilon_a|}\right)^{\frac{1}{2}}$, so that the critical voltage is really sensitive to the value of the anchoring coefficient W. Adsorption of kunipia particles at the smectic–glass interface might mitigate the surface anchoring and thus reduce the value of U^{**} in doped materials, as the experimental data suggest.

6. Conclusion

We have monitored nucleation and expansion of domains in a homeotropic SmA cell under the action of an electric field that reorients the molecules parallel to the plane of the cell. The reorientation occurs via nucleation of TFCDs. The initial stage of TFCD formation, when the radius is close to the critical radius of nucleation a^* is hard to monitor, since a^* is very small, in the micron or even sub-micron range. By the time the TFCD is visible, the nucleation has already occurred. We employed the newly developed FCPM technique to demonstrate that the circular base of the visible TFCD can be located in the bulk of the sample, suggesting that nucleation of TFCDs can take place in the bulk. As the appearance of a TFCD from an ideal non-distorted smectic structure requires a huge energy barrier to be overcome, nucleation cannot be a homogeneous process; it is facilitated by imperfections such as doping nanoparticles, edges of the sample, etc. The presence of clay nanoparticles can reduce the energy barrier for nucleation by increasing the ground state energy due to the distortion of layers. Our experiments confirm that in the doped cells, TFCDs develop at lower voltages than in cells filled with a pure smectic material.

The radius of the appearing TFCDs increases with the applied voltage; the domains preserve their circular shape. However, as the radius of the domain reaches some second critical value a^{**}, their shape becomes irregular. Further expansion of the reoriented texture can be modelled as elongation of a SD emerging from the parent TFCD rather than as an enlargement of the TFCD. Although the real structural transformation of

a TFCD is rather complex, the simple SD model explains it at least qualitatively. The main reason for the TFCD–SD transformation is the surface anchoring. In an expanding TFCD, the SmA layers make a progressively larger angle with the anchoring-imposed orientation, $\theta \rightarrow \pi/2$, as the TFCD radius increases. In an elongating SD, the nearly constant width ρ_s limits the maximum tilt of the SmA layers from the anchoring-imposed alignment, $\theta = \arctan \rho_s$, $\theta < \pi/2$. Therefore, elongation via SD is energetically preferable over the uniform expansion of TFCDs when the surface anchoring is non-zero, despite the fact that the elastic cost of the SD is high because the central SD plane is a plane defect of the tilt grain boundary defect type. The quantitative SD model demonstrates indeed that above some critical voltage U^{**}, there is a range of SD widths for which the SD line tension becomes negative, implying that these domains will grow by increasing their length. The range of the SD widths for which the energy is negative is rather broad for any $U > U^{**}$, which explains the highly irregular growth pattern after the TFCD reaches the radius a^{**}. In the doped cell, the transition TFCD–SD occurs at somewhat lower voltages than in the pure cell, which might be related to the mitigation of anchoring at the smectic–glass interface caused by adsorption of nanoparticles. As the temperature increases, the critical radius a^{**} becomes larger, as the surface anchoring becomes weaker.

S. G. would like to acknowledge support from NSF grant DMR 9704579 and K.P. from NSF REU grant DMR 9619406. O.D.L. was partially supported by donors of the Petroleum Research Fund, administered by the ACS, grant 35306-AC7, NSF STC ALCOM grant DMR89-20147, and by a research grant from Rockwell Science Center.

References

[1] KLEMAN, M., and LAVRENTOVICH, O. D., 2003, *Soft Matter Physics: An Introduction*, (Springer, New York).
[2] LI, Z., and LAVRENTOVICH, O. D., 1994, *Phys. Rev. Lett.*, **73,** 280.
[3] LAVRENTOVICH, O. D., KLEMAN, M., and PERGAMENSHCHIK, V. M., 1994, *J. Phys. II (Fr.)*, **4,** 377.
[4] KAWASUMI, M., HASEGAWA, N., USUKI, A., OKADA, A., and KURAUCHI, T., 1996, in *Proceedings of Liquid Crystals for Advanced Technologies*, p. 311; Kawasumi, M., Hasegawa, N., Usuki, A., and Okada, A., 1999, *Appl. Clay Sci.*, **15,** 93.
[5] SMALYUKH, I. I., SHIYANOVSKII, S. V., and LAVRENTOVICH, O. D., 2001, *Chem. Phys. Lett.*, **336,** 88.
[6] BOIKO, V. G., MOGEL, KH. I., SYSOEV, V. M., and CHALYI, A. V., 1991, *Usp. Fiz. Nauk* **161,** 77; *Sov. Phys. Usp.* **34,** 141.
[7] PERSHAN, P. S., and PROST, J., 1974, *J. appl. Phys.*, **46,** 2343.
[8] FRIEDEL, G., 1922, *Ann. Phys. (Paris)*, **18,** 273.
[9] KLEMAN, M., and LAVRENTOVICH, O. D., 2000, *Eur. Phys. J. E*, **2,** 47.
[10] AVRAMI, M., 1939, *J. chem. Phys.*, **7,** 1103; AVRAMI, M., 1940, *J. chem. Phys.*, **8,** 212.
[11] ERUKHIMOVITCH, V., and BARAM, J., 1994, *Phys. Rev. B*, **50,** 5854.
[12] LI, Z., FOLKS, W. R., and LAVRENTOVICH, O. D., 1994, *Proc SPIE*, **2175,** 21.
[13] KLEMAN, M., 1983, *Points, Lines, and Walls in Liquid Crystals, Magnetic Systems and Various Ordered Media* (New York: Wiley).
[14] LAVRENTOVICH, O. D., and YANG, D.-K., 1998, *Phys. Rev. E*, **57,** R6269.